Global fast non-singular terminal sliding-mode control for high-speed nanopositioning

Geng Wang[a,c], Yongsheng Zhou[c], Lei Ni[a], Sumeet S. Aphale [b,*],

[a] *Key Laboratory of Testing Technology for Manufacturing Process of Ministry of Education, Southwest University of Science and Technology, Mianyang, China, 621010*

[b] *Artificial intelligence, Robotics and Mechatronic Systems Group (ARMS), School of Engineering, University of Aberdeen, Aberdeen, UK, AB243UE*

[c] *School of Mechanical and Power Engineering, Henan Polytechnic University, Jiaozuo, China, 454003*

Abstract

This paper presents a new Global Fast Non-singular Terminal Sliding Mode Controller (GFNTSMC) that delivers high-precision tracking of high-frequency trajectories when applied to a piezo-driven nanopositioner. The control scheme is realized by combing inverse hysteresis model and global fast non-singular terminal sliding mode compensation. The inverse Bouc-Wen hysteresis model is used to calculate the required hysteresis-compensating feedforward control voltage according to the reference signal. The key uniqueness of the proposed control strategy is it's red global fast convergence, achieved with high accuracy and high bandwidth. The stability of the reported GFNTSMC controller is proved with the Lyapunov theory. Its performance is verified through experimentally recorded tracking results, and its superiority over three benchmark control approaches, namely the Proportional-Integral-Derivative (PID), the Positive Position Feedback with integral action (PPF+I) and the conventional linear high-order sliding mode controller (LHOSMC) is demonstrated through comparative tracking error analysis. Its wide-band stability as well as its significant robustness to parameter uncertainty is also showcased.

Keywords: Nanopositioning, Sliding-mode control, Trajectory tracking, High order sliding surface, global fast non-singular SMC

1. Introduction

Precision positioning platforms driven by piezoelectric actuators have drawn significant research interest in recent years and have been widely used in a range of applications including micro/nano-positioning stages [1], micromanipulators [2], microinjection system [3], fast steering mirrors [4], fast tool servo [5], etc. Piezoelectric actuation possesses several advantages over other kinds of drives viz: large output force, high resolution, high operation bandwidth, simplicity of design and system integration. However, the positioning performance of piezo-actuated nanopositioners is severely affected by the inherent hysteresis nonlinearity [6], multiple lowly-damped resonance modes, and other disturbances [7] including cross-axial coupling [8] and creep. In order to tackle these problems, various control approaches have been proposed to meet the high-precision and high-speed requirements in precision positioning applications [9, 10]. Due to the inherent linear and nonlinear dynamics of a nanopositioning system and the stringent performance requirements and high-bandwidth desired trajectories (typically triangular and staircase / ramp signals to generate a raster pattern), developing relevant control strategies is a significantly challenging task [11]. Initial efforts focussed on addressing the positioning errors and tracking bandwidth limitations arising from the linear dynamics alone - the lowly damped, relatively low frequency resonance that dominates the frequency response of most nanopositioning axes. Open-loop efforts led this track via dynamic inversion or notch filter integration approaches [12]. Due to lack of robustness, high dependency on accurate modeling and low disturbance rejection characteristics, open-loop approaches were discarded in favour of closed-loop approaches [13]. Closed-loop approaches predominantly focussed on a two stage approach of implementing linear damping and tracking controllers in tandem to de-

*Corresponding author, e-mail: s.aphale@abdn.ac.uk

liver acceptable positioning performance [14]. However, most of the reported techniques are based on a simple second-order system model and do not explicitly model the hysteresis; rather depend on the high-gain tracking controller (typically an integrator) to minimize hysteresis-induced positioning errors.

In the recent years, nonlinear control techniques, especially Sliding-Mode Control (SMC) schemes [15, 16] have demonstrated significant performance improvement over linear controllers [17, 3]. Asymptotic convergence of tracking errors can be achieved in traditional SMC based on a linear sliding mode manifold [18]. In the above-mentioned work, traditional linear sliding mode can only guarantee infinite convergence time. Terminal Sliding-mode control (TSMC) employs nonlinear sliding hyperplane and can achieve finite-time convergence, which is of great significance for improving the positioning performance of a nanopositioning system. The traditional TSMC typically is singular and consequently, the non-singular TSMC (NTSMC) scheme has been proposed in [19] which can eliminate the existing singular problem in traditional TSMC. However, when the system state is far away from the equilibrium point, the convergence speeds of both TSMC and NTSMC are lower than that of the traditional linear SMC. Moreover, chattering exists in TSMC and NTSMC due to discontinuity in the control. To alleviate this issue, researchers have proposed a Fast TSMC (FTSMC) that essentially inhibits chattering and converges faster - however, it has a singular problem. Consequently, non-singular FTSMC has been put forward which can essentially eliminates chattering and does not have a singularity problem [20]. At present, there are several NFTSMC methods reported in literature [21, 22]. Literature [21] puts forward a new NFTSMC concept whose basic principle is showed based on some new forms of FTSMC. However, only the theoretical and simulation results in [21] are not enough for piezoelectric-positioning application. Literature [22] used a FNTSMC method to realize a robust controller for a second-order linear motor model. But this work in [22] is not suitable for high-order dynamics systems. The common features of these methods are: absence of chattering, absence of singularity, and short, finite time convergence. Though its chatter-free property combined with fast error convergence is highly desirable, the successful application of the NFTSMC technique on a nanopositioner is hitherto unexplored.

Several previous works demonstrate the significant benefits nonlinear SMC has in the control and consequent performance improvement of nanopositioners due to the nonlinear hysteresis as well as the unmodeled high-bandwidth dynamics, [23, 24, 25]. This is a key motivations in employing the NFTSMC. Inspired by a fast terminal attractor [26] and a recursive design method [27], this work proposes a new recursive non-singular fast terminal sliding manifold intended for high-order piezoelectric systems that leads to a novel NFTSM controller. The advantages of the proposed SMC controller include: 1) The proposed control scheme can deal with uncertainties both in the linear and nonlinear controlled plants. 2) it is an ideal control scheme for complex higher-order nonlinear dynamic plants, such as piezoelectric nanopositioning stages that suffer parametric uncertainties, un-modelled high-order dynamics, external perturbations, and hysteresis nonlinearities. 3) It provides a systematic approach to the problem of maintaining stability and consistent performance especially in applications where traditionally popular controllers such as PID may fail due to uncertain environments. 4) A key advantage of the proposed control scheme is the fast convergence of system state in the *g*lobal sense. Moreover, this non-singular, chatter-free, terminal sliding mode control method with global fast convergence (GNFTSMC), is based on the full, high-order model of the nanopositioner axis' in-bandwidth dynamics and not the truncated low-order model - thereby achieving significantly superior performance compared to other reported methods.

A combined feedforward - feedback control scheme capable of improving the positioning performance of a nanopositioner is proposed, where a new high-order, non-singular, fast terminal sliding manifold and a double power reaching law based on Lyapunov theory is formulated. This is further combined with an inverse Bouc-Wen hysteresis model to povide superior hysteresis compensation. In addition to a new recursive SMC control design scheme for the full, high-order model of the nanopositioner axis' in-bandwidth dynamics, a non-singular, chatter-free, terminal SMC controller with fast convergence of system state in the global sense is also developed and experimentally validated. The major contribution of this work is the design, analysis and experimental validation of the novel GNFTSMC scheme for nanopositioning applictions. The key desirable properties of the proposed control method are:

- The control signal is continuous as long as the n^{th}-order derivative of the reference is continuous, guaranteeing a chatter-free operation; thereby improving both tracking precision and actuator lifetime.

- The proposed GNFTSMC design guarantees finite-

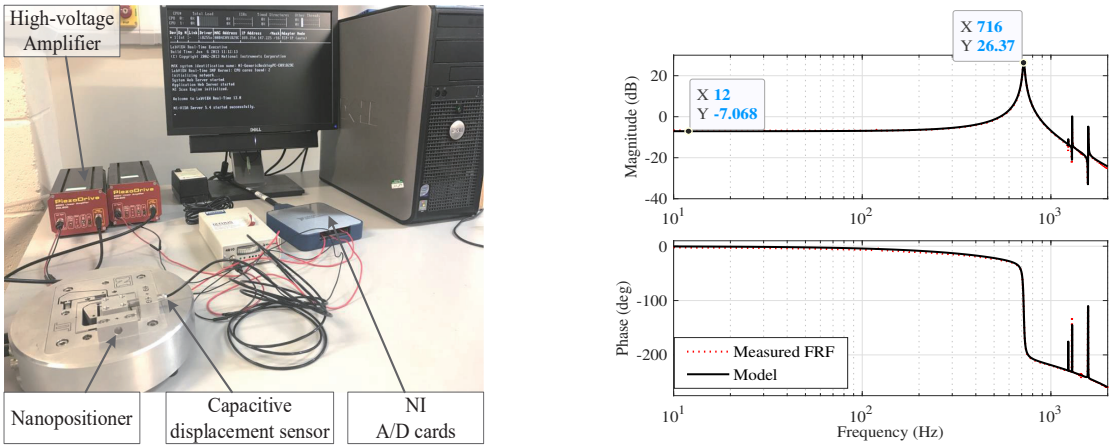

(a) (b)

Figure 1: (a) The experimental setup used in this work showing the two-axis, serial kinematic, piezoelectrically actuated nanopositioner, the high-voltage amplifiers, the capacitive displacement sensor and the computer embedded with NI A/D cards and LabView. (b) Measured magnitude response of the system ($\cdots$) and the magnitude response of the full linear model (—) adopted in this work showing excellent acuracy in capturing the linear in-bandwidth dynamics.

time convergence in the presence of modeling errors, deeming the system robust to parameter uncertainties.

- Irrespective of where the initial state of the system is located in the phase-plane, the proposed sliding mode controller can always drive the system state to the equilibrium point quickly. In other words, it can convergence to the equilibrium point very fast in both the sliding stage and the reaching stage. On the reaching stage, state of the system has a fast convergence speed while going away from or approaching the sliding surface. It also has a property of fast convergence on the sliding surface, where it converges exponentially if near equilibrium, and in power form if away from equilibrium. The proposed controller has a fast convergence property in the global sense, so to speak.

2. System Modeling and Open-loop Response

The experimental setup used in this work is shown in Fig.1(a). It consists of a piezo-stack actuated, flexure-guided, two-axis (x - y) nanopositioner. Each axis of the nanopositioner is driven by a 10 mm, 200 V piezoelectric stack actuator capable of producing 40 μm motion along each axis. The nanopositioner also provides integrated mounts for capacitive sensor probes. The MicroSense 6810 capacitive displacement sensor and 6504-01 probe with a sensitivity of 5 mm/V provides a voltage signal proportional to the displacement sensed along each axis. The piezoelectric stack actuators are supplied with both AC actuation and DC bias voltages by two PiezoDrive PDL200 voltage amplifiers with a gain of 20.

2.1. Modeling the linear dynamics

In order to identify the linear dynamics of one axis of the nanopositioner, small signal frequency response functions (FRFs) were recorded for the x-axis. The FRFs are obtained by applying a sinusoidal chirp signal (from 10 to 1500 Hz) with an amplitude of 0.2 V as input to the voltage amplifier of the x-axis and measuring the output signal (sensor voltage proportional to axial displacement) along the same axis. Subsequently, the FRF is computed by taking the Fourier transform of the recorded data. The sampling frequency of the A/D system is set to 20 kHz. As seen from the magnitude response presented in Fig.1(b), the dynamics within the recorded bandwidth-of-interest are dominated by the lowly-damped resonant peak occurring at 716 Hz (which towers in magnitude over the entire bandwidth-of-interest).

Using the popular modeling technique employed extensively in relevant literature [28], the measured frequency response of the axis shown in Fig.1(b), is modeled as a summation of a number of second-order transfer functions, to account for the resonances, combined with a Pad'e approximation of the system's inherent delay manifesting as an additional phase contribution at higher frequencies. The overall transfer function model is 10^{th}-order. However, as the control strategy

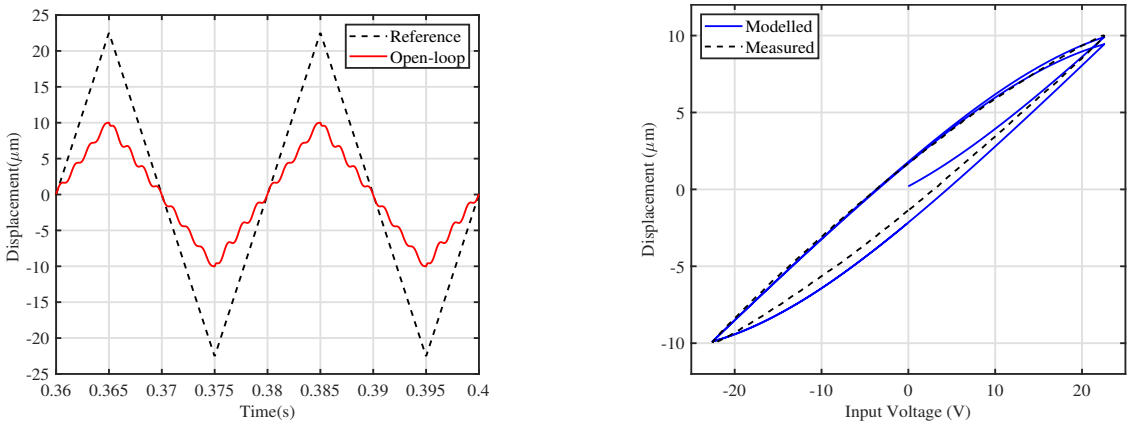

(a) (b)

Figure 2: (a) The reference input (50 Hz Triangle wave) and the recorded output clearly showing the resonance-induced high-frequency errors and hysteretic effects of the piezo-actuated nanopositioner axis. (b) The measured (- -) and modeled (—) hysteresis loops clearly demonstrating the good agreement between the actual system and the model.

adopted herewith is of the sliding-mode type, the identified transfer function is converted into a differential equation relating the input and output that can be parametrically written as:

$$y^{(n)}(t) + \sum_{k=0}^{n-1} a_k y^{(k)}(t) = \sum_{k=0}^{m} b_k u^{(k)}(t) \qquad (1)$$

where, $u(t)$ is the input voltage applied to the platform as a function time t; $y(t)$ is the displacement produced along the axis; $u^{(k)}(t)$ and $y^{(k)}(t)$ are respectively the kth derivatives of $u(t)$ and $y(t)$; m and n are the orders of the model, and $m < n$; a_k and b_k are constant coefficients of the model.

To validate the identified model, the magnitude response of the model was superimposed on that of the nanopositioner's axis, see Fig.1(b). Clearly, the identified model is a very accurate match to the measured linear dynamics of the nanopositioner axis. The effect of reference inputs's high frequency components exciting the resonant dynamics of the system is clearly visible in the measured time-domain response of the axis to a 50 Hz triangular wave reference input, see Fig.2(a).

2.2. *Modeling the hysteresis nonlinearity*

Hysteresis is the nonlinear behaviour inherent to the piezo-stack actuator employed by the nanopositioner. the hysteresis curve of the nanopositioner axis was obtained by plotting the input reference and output displacement signals for a 1 Hz, ± 10 μm sinusoidal displacement, as shown in Fig.2(b). Due to its apparent simplicity, its ability to capture the nonlinear behaviour accurately and its popularity, the Bouc-Wen model has been adopted in this work. The Bouc-Wen hysteresis model can be generally expressed as follows [29]:

$$\begin{cases} H(t) = du - h \\ \dot{h} = \alpha_1 \dot{u} - \alpha_2 |\dot{u}| h - \alpha_3 \dot{u} |h| \end{cases} \qquad (2)$$

where, $H(t)$ is the hysteresis displacement; d is piezoelectric constant; h is an intermediate state variable whose time derivative is $\dot{h}$; α_1, α_2 and α_3 are the coefficients that determine the shape and orientation of the hysteresis loop, the symbol $|\cdot|$ denotes the absolute value function. After a thorough numerical search, the Bouc-Wen hysteresis model parameters were selected to be: d=3.2; α_1=1.3; α_2=0.6; α_3= 0.05. As seen in Fig.2(b), the adopted hysteresis model captures the nonlinear hysteresis on the axis relatively well. There are some clearly visible discrepancies between the measured and the modeled hysteresis loops. However, the subsequently proposed control design will address this as a disturbance and compensate for this discrepancy adequately.

Combining the linear and the nonlinear models, the entire dynamic model of one axis of the nanopositioner can be expressed as:

$$y^{(n)}(t) + \sum_{k=0}^{n-1} a_k y^{(k)}(t) + H(t) + \Delta = \sum_{k=0}^{m} b_k u^{(k)}(t) \qquad (3)$$

where, Δ is the uncertain displacements caused by all the un-modelled (out-of-bandwidth) dynamics and disturbances and it is bounded as: $|\Delta| \leqslant \bar{\Delta}$.

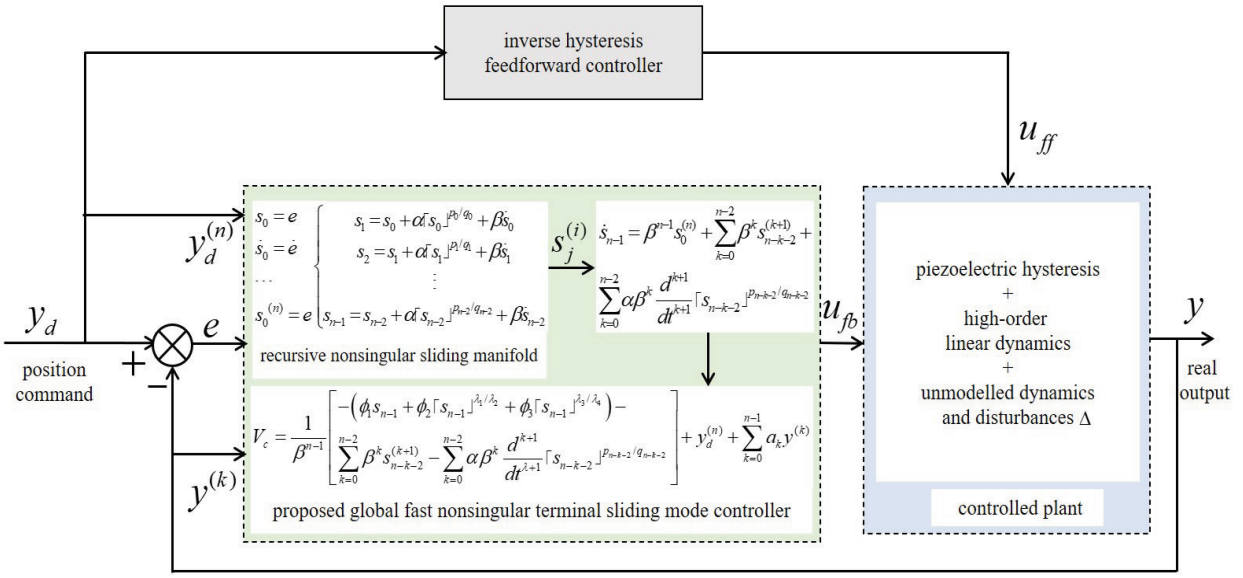

Figure 3: Block-diagram of the proposed control scheme showing the overall signal flow.

3. Controller Design

The control objective is to track a scanning trajectory (typically triangular in nature) accurately, in the presence of unknown, external disturbances. In this work, a feedforward hysteresis compensation scheme combined with a global fast nonsingular terminal sliding-mode based feedback control scheme is proposed. It is shown that the proposed control scheme drives the positioning error to convergence within a bounded region, in finite time. The block diagram of the control system is shown in Fig.3. The central premise of the proposed control scheme is to incorporate a relatively accurate inversion of the identified hysteresis, such that the hysteresis-compensated system can be quite accurately approximated by a linear system. The in-bandwidth model matching imperfections as well as unmodelled out-of-bandwidth dynamics can then be aggregated and considered as a disturbance. These disturbances can then be addressed effectively via the proposed non-singular, terminal sliding-mode controller implemented in a feedback loop.

3.1. Inverse Bouc-Wen feedforward controller

To design the feedforward controller, an inverse hysteresis scheme, similar to the one proposed in [30], is utilized. The overall concept is shown in Figure 4, clearly presenting the relationship between the inverse feedforward controller and the hysteresis model output. According to Eq.(2), the feedforward controller u_{ff} is designed as following

$$u_{ff} = \frac{1}{d}(y_d + h) \tag{4}$$

where, h can be calculated by Eq.(2), y_d is the command position.

3.2. Global fast nonsingular TSMC feedback controller

In this subsection, the controller input $u(t)$ is first designed under the assumption that the disturbance $\Delta = 0$, ensuring that the control law will converge to zero in finite time. Subsequently, the convergence and robustness of the designed system with nonzero disturbance ($\Delta \neq 0$) will be analyzed. It will be demonstrated that, when the disturbance is not zero and is bounded by an upper bound, the control law will converge to a region proximal to the equilibrium point.

If the position tracking error is defined as:

$$e = y - y_d \tag{5}$$

where, y is the output displacement, and the y_d is the desired displacement. Then, the derivatives of the tracking error can be written as:

$$\begin{aligned} \dot{e} &= \dot{y} - \dot{y}_d \\ \ddot{e} &= \ddot{y} - \ddot{y}_d \\ &\vdots \\ e^{(n)} &= y^{(n)} - y_d^{(n)} \end{aligned} \tag{6}$$

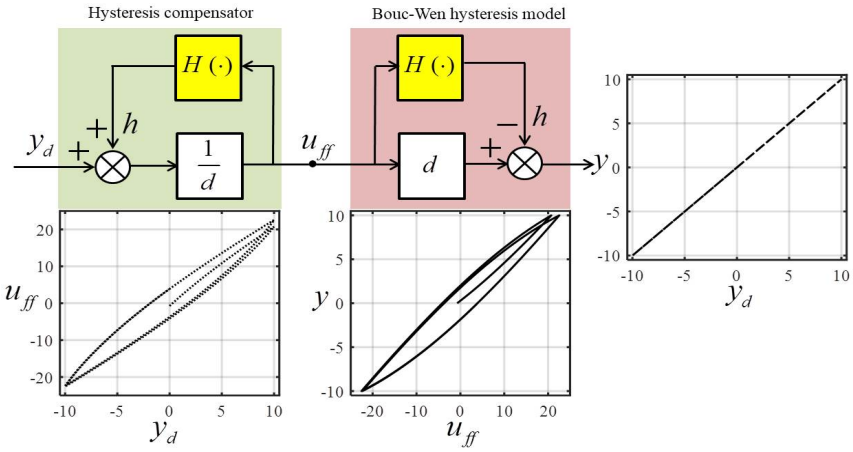

Figure 4: Block-diagram and relevant block outputs for the inverse-hysteresis compensation adopted in this work.

Then, consecutive states can be initialized as follows:

$$s_0 = e, \quad \dot{s}_0 = \dot{e}, \quad \cdots, \quad s_0^{(n)} = e^{(n)} \tag{7}$$

Inspired by a fast terminal attractor with singularity property [26] and a recursive design method [27], this work proposes a new recursive non-singular fast terminal sliding manifold which is defined as follows:

$$\begin{cases} s_1 = s_0 + \alpha \lceil s_0 \rfloor^{p_0/q_0} + \beta \dot{s}_0 \\ s_2 = s_1 + \alpha \lceil s_1 \rfloor^{p_1/q_1} + \beta \dot{s}_1 \\ \vdots \\ s_{n-1} = s_{n-2} + \alpha \lceil s_{n-2} \rfloor^{p_{n-2}/q_{n-2}} + \beta \dot{s}_{n-2} \end{cases} \tag{8}$$

Here, $\alpha, \beta \in \mathrm{R}^+$; p_j, q_j are constant positive odd numbers with $j = 1, 2, \cdots, n-1.$; $1 < n-j < \frac{p_{j-1}}{q_{j-1}} < n-j+1$ can guarantee the non-singularity property. It is worth noting that $\frac{p_{j-1}}{q_{j-1}} > 1$, this kind of selection of the value of $\frac{p_{j-1}}{q_{j-1}}$ is different from that in [27], and makes it easy to design in practice. In this work the formula $\lceil \bullet \rfloor^r = |\bullet|^r \operatorname{sign}(\bullet)$ is used, where $\bullet \in R$ and $r \in R$. The symbol $\lceil \bullet \rfloor^r$ here is to perform the calculation on the right-hand side of the formula as in the literature [31, 32]. And it is a smooth and monotonically increasing function and will always return a real number. Specially, we will get $\lceil \bullet \rfloor^{p/q} = |\bullet|^{p/q} \operatorname{sign}(\bullet)$ if $r = p/q$, where both p and q are positive odd integers in this paper. In addition, the symbol sign(·) denotes the Signum Function.

From Eq.(8), the i-th derivative of s_j can be written as:

$$s_j^{(i)} = s_{j-1}^{(i)} + \alpha \frac{d^i}{dt^i} \lceil s_{j-1} \rfloor^{p_{j-1}/q_{j-1}} + \beta s_{j-1}^{(i+1)} \quad (i \in \mathrm{N}^+) \tag{9}$$

Taking the derivative of s_{n-1} recursively according to Eq.(9) results in:

$$\begin{aligned} \dot{s}_{n-1} &= \dot{s}_{n-2} + \alpha \tfrac{d}{dt} \lceil s_{n-2} \rfloor^{p_{n-2}/q_{n-2}} + \beta s_{n-2}^{(2)} \\ &= \dot{s}_{n-2} + \alpha \tfrac{d}{dt} \lceil s_{n-2} \rfloor^{p_{n-2}/q_{n-2}} + \\ &\beta \left[s_{n-3}^{(2)} + \alpha \tfrac{d^2}{dt^2} \lceil s_{n-3} \rfloor^{p_{n-3}/q_{n-3}} + \beta s_{n-3}^{(3)} \right] \\ &= \beta^{n-1} s_0^{(n)} + \textstyle\sum_{k=0}^{n-2} \beta^k s_{n-k-2}^{(k+1)} + \\ &\textstyle\sum_{k=0}^{n-2} \alpha \beta^k \frac{d^{k+1}}{dt^{k+1}} \lceil s_{n-k-2} \rfloor^{p_{n-k-2}/q_{n-k-2}} \end{aligned} \tag{10}$$

For simplicity, an intermediate variable is defined as:

$$V_c = \sum_{k=0}^{m} b_k u^{(k)} \tag{11}$$

Then, the controlled plant Eq.(3) becomes:

$$y^{(n)} + \sum_{k=0}^{n-1} a_k y^{(k)} = V_c \tag{12}$$

Theorem 3.1. *For the controlled plant given in Eq.(12), if the sliding manifold is designed detailed in Eq.(8) and the control law given in Eq.(13) is selected, then the control system is stable and the tracking error as given by Eq.(5) will converge to a small neighborhood of zero in finite time.*

Proof. The proposed control law is given by:

$$\begin{aligned} V_c = \tfrac{1}{\beta^{n-1}} \Big[&- \left(\phi_1 s_{n-1} + \phi_2 \lceil s_{n-1} \rfloor^{\lambda_1/\lambda_2} + \phi_3 \lceil s_{n-1} \rfloor^{\lambda_3/\lambda_4} \right) - \\ &\textstyle\sum_{k=0}^{n-2} \beta^k s_{n-k-2}^{(k+1)} - \sum_{k=0}^{n-2} \alpha \beta^k \frac{d^{k+1}}{dt^{k+1}} \lceil s_{n-k-2} \rfloor^{p_{n-k-2}/q_{n-k-2}} \Big] \\ &+ y_d^{(n)} + \textstyle\sum_{k=0}^{n-1} a_k y^{(k)} \end{aligned} \tag{13}$$

where, $\phi_1, \phi_2, \phi_3 \in \mathbb{R}^+$ are all positive constants and λ_i for $(i = 1, 2, 3, 4)$ are constant positive odd numbers such that, $\lambda_1/\lambda_2 > 1$, $0 < \lambda_3/\lambda_4 < 1$.

As reference input trajectories are predefined, it follows that higher-order derivatives $v_d^{(n)}$ of reference are available (computable). Combining Eq.(10) and Eq.(13) yields

$$V_c = \frac{1}{\beta^{n-1}}\left[-\left(\phi_1 s_{n-1} + \phi_2 \lceil s_{n-1} \rfloor^{\lambda_1/\lambda_2} + \phi_3 \lceil s_{n-1} \rfloor^{\lambda_3/\lambda_4}\right) + \beta^{n-1} s_0^{(n)} - \dot{s}_{n-1}\right] + y_d^{(n)} + \sum_{k=0}^{n-1} a_k y^{(k)} \tag{14}$$

As $y^{(n)} - y_d^{(n)} = s_0^{(n)}$, substituting Eq.(14) into the controlled plant given in Eq.(12) results in:

$$\dot{s}_{n-1} = -\left(\phi_1 s_{n-1} + \phi_2 \lceil s_{n-1} \rfloor^{\lambda_1/\lambda_2} + \phi_3 \lceil s_{n-1} \rfloor^{\lambda 3/\lambda_4}\right) \tag{15}$$

Selecting the following Lyapunov candidate function:

$$V = 0.5 s_{n-1}^2 \tag{16}$$

and combining Eq.(15) results in:

$$\begin{aligned} \dot{V} &= s_{n-1}\dot{s}_{n-1} \\ &= -\left(\phi_1 s_{n-1}^2 + \phi_2 \lceil s_{n-1} \rfloor^{(\lambda_1+\lambda_2)/\lambda_2} + \phi_3 \lceil s_{n-1} \rfloor^{(\lambda_3+\lambda_4)/\lambda_4}\right) \end{aligned} \tag{17}$$

As $(\lambda_1 + \lambda_2)$ and $(\lambda_3 + \lambda_4)$ are even numbers:

$$\dot{V} < 0 \tag{18}$$

It is clear from Eq.(15), that s_{n-1} is the only equilibrium point. Thus, Eq.(18) signifies that the sliding surface s_{n-1} will be reached in finite time [33]. In addition, s_{n-1} will eventually reach a tiny neighborhood near the equilibrium, so $\dot{V}$ will not be zero. Consequently, stability of the system can be guaranteed.

It should be noted that Eq.(15) is a double power reaching law. Thus, the Gauss' Hypergeometric function [34] can be used to calculate the sliding mode reaching time. By solving Eq.(15), the reaching time for $s_{n-1} = 0$ can be obtained. Once the state trajectory reaches $s_{n-1} = 0$; it will be confined to the sliding manifold. Then, from the recursive sliding manifold given in Eq.(8), it can be concluded that $s_{n-2}, s_{n-3}, \cdots, s_0$ will reach equilibrium subsequently as long as s_{n-1} reaches equilibrium. Consequently, the position tracking error given by Eq.(5) will eventually reach a small region. It should be noted that the tracking error will also reach a small region in finite time due to the terminal sliding manifold given in Eq.(8). □

After the control law in Eq.(13) is formalized, V_c is a known variable. From Eq.(11), $u(t)$ can be obtained after V_c is filtered through $\frac{1}{b_m s^m + b_{m-1} s^{m-1} + \cdots + b_1 s + b_0}$. This yeilds the following feedback control law u_{fb}:

$$u_{fb} = V_c * \frac{1}{b_m s^m + b_{m-1} s^{m-1} + \cdots + b_1 s + b_0} \tag{19}$$

Robustness analysis: With the assumption that the disturbance Δ can be freely chosen while designing the control law u_{fb}, analyzing the robustness of the control law for nonzero disturbance is essential. The modeling errors and unknown exogenous disturbances will impact the speed of convergence. Moreover, the steady-state tracking trajectory can only be made to reach a small neighbourhood of the equilibrium, but never converged to the equilibrium. In other words, robustness of the control algorithm expectedly comes at the cost of a minimal loss in positioning accuracy. To formally analyze the robustness to of the proposed feedback control law, the system Eq.(3) which includes unknown disturbances is further explored.

Substituting Eq.(11) into Eq.(3) yields:

$$y^{(n)}(t) + \sum_{k=0}^{n-1} a_k y^{(k)}(t) + \Delta = V_c \tag{20}$$

Also, substituting Eq.(14) into Eq.(20) yields:

$$\dot{s}_{n-1} = -\left(\phi_1 s_{n-1} + \phi_2 \lceil s_{n-1} \rfloor^{\lambda_1/\lambda_2} + \phi_3 \lceil s_{n-1} \rfloor^{\lambda_3/\lambda_4} + \Delta\right) \tag{21}$$

To ensure convergence, the criteria, $s_{n-1}\dot{s}_{n-1} < 0$, needs to be satisfied. In other words, $\text{sign}(s_{n-1})\dot{s}_{n-1} = \frac{s_{n-1}\dot{s}_{n-1}}{|s_{n-1}|} < 0$ must be satisfied. This can be further expanded as follows:

$$\begin{aligned} &\text{sign}\,(s_{n-1})\,\dot{s}_{n-1} \\ &= -\left(\phi_1 |s_{n-1}| + \phi_2 |s_{n-1}|^{\lambda_1/\lambda_2} + \right. \\ &\left. \phi_3 |s_{n-1}|^{\lambda_3/\lambda_4} + \text{sign}\,(s_{n-1})\,\Delta\right) \\ &\leq -\left(\phi_1 |s_{n-1}| + \phi_2 |s_{n-1}|^{\lambda_1/\lambda_2} + \phi_3 |s_{n-1}|^{\lambda_3/\lambda_4} - \bar{\Delta}\right) \\ &< 0 \end{aligned} \tag{22}$$

Consequently,

$$\bar{\Delta} < \phi_1 |s_{n-1}| + \phi_2 |s_{n-1}|^{\lambda_1/\lambda_2} + \phi_3 |s_{n-1}|^{\lambda_3/\lambda_4} \tag{23}$$

Thus, Eq.(23) provides the constraint condition for disturbance Δ. If ϕ_1, ϕ_2 and ϕ_3 are large enough, and appropriate $\lambda_1, \lambda_2, \lambda_3, \lambda_4$ are selected, the convergence neighborhood can be made arbitrarily small. The convergence of state s_{n-1} reaching a small neighborhood of zero can then be formalized as:

$$\Delta = \left\{s_{n-1} : \phi_1 |s_{n-1}| + \phi_2 |s_{n-1}|^{\lambda_1/\lambda_2} + \phi_3 |s_{n-1}|^{\lambda_3/\lambda_4} \leq \bar{\Delta}\right\} \tag{24}$$

As a result, the system tracking performance during the reaching phase depends on the choice of $\phi_1, \phi_2, \phi_3, \lambda_1, \lambda_2, \lambda_3, \lambda_4$.

Remark 1: The proposed non-singular terminal sliding-mode feedback controller has a global fast convergence property. At the reaching stage, a double power reaching law given by Eq.(15) can guarantee that the state s_{n-1} has a fast bi-directional convergence to the sliding manifold. At the sliding stage, the recursively designed fast sliding manifold given in Eq.(8) can guarantee the system state converges exponentially if near equilibrium, and converges via a power law, if away from equilibrium. It should be noted that, what we designed is a "global fast" terminal sliding mode controller, not a kind of classical "global" sliding mode controller which was firstly proposed by Yu-Sheng Lu [35] in 1995. As stated in paper [36], "global fast terminal sliding mode control can have a fast convergence speed in the whole convergence process". Paper [37] also presents a "global fast" terminal sliding mode control scheme. In this work, we emphasize the "global fast" as a whole concept, which indicates that the designed controller has a fast convergence speed in the global state space.

Remark 2: In this work, the feedforward control law u_{ff} is aimed at hysteresis compensation, and the feedback control law is aimed at controlling the system's linear dynamics (resonance damping and input tracking). When the actual nanopositioning platform is controlled, the total control law is $u = u_{ff} + u_{fb}$. According Eq.(4), we can see that feedforward controller is continuous. Thus, the total control law is continuous as long as ${s^{(k+1)}}_{n-k-2}$ and $\frac{d^{k+1}}{dt^{k+1}}\lceil s_{n-k-2} \rfloor^{p_{n-k-2}/q_{n-k-2}}$ $(k = 0, 1, ..., n-2)$ are continuous. This is guaranteed as long as the *nth* order derivative of the reference signal is continuous. Furthermore, as the *nth* $(n \geq 2)$ order derivatives for a triangular trajectory are all zero, this law also guarantees accurate chattering-free tracking for triangular trajectories.

Remark 3: It should be noted that the calculation of $\frac{d^{k+1}}{dt^{k+1}}\lceil s_{n-k-2} \rfloor^{p_{n-k-2}/q_{n-k-2}}$ in Eq.(13) may be complex for a practicing engineer to effectively develop and synthesize this controller. To ease this difficulty, a general formula to calculate $\frac{d^n}{dt^n}\lceil s \rfloor^r$ ($r > n$ is the ratio of two positive odd numbers) is provided in the Appendix. The readers of this paper can also email the authors to get the derived formula and the corresponding MATLAB code.

Tracking performance as well as robustness of the proposed GNFTFSM control law is experimentally validated on a piezoelectric nanopositioner axes. Results and disussion are presented in the following section.

4. Experimental Results and Discussion

The nanopositioner typically has both linear dynamics due to its mechanical structure and nonlinear hysteresis dynamics due to the piezo-actuator, as shown in our previous work [38, 39, 40]. Typically, the linear dynamics can be accurately modeled in the frequency-domain via a summation of second-order transfer functions (one for each resonant mode) [41, 42, 43] while the hysteresis can be modeled via a kind of hysteresis model, such as Bouc-Wen model [44], Prandtl-Islinskii model [45], Preisach model [46]. In the time-domain, the linear dynamics can be written as Eq.(1) while the hysteresis can be modeled as given in Eq.(2). The inherent system delay can be approximated using the Pade' approximation [47].

Here, it is better to talk about how to use the controller in practice. As we know, the sliding mode controller can easily be programmed into a rapid prototyping system such as dSPACE system [48, 49], PC-based development system with an xPC target [50] or a LabVIEW real-time target [12] and NI data acquisition card, a FPGA based LabVIEW development system [51, 52]. In this paper, the experiments presented here were conducted on the LabVIEW real-time target which is the same as in the literature [12, 39]. Other similar implementations of nonlinear sliding-mode controllers have already been reported in literature [52, 53]. This is not a major complexity or inconvenience, given the performance improvement.

The experimental setup employed in this paper is shown in Fig.1(a). A PCI-6621 data acquisition card from National Instruments installed on a PC running the Real-Time Module from LabVIEW is used to interface between the experimental platform and the control design. The PC utilized is an OPTIPLEX 780 with an Intel(R) Core(TM)2 Duo Processor running at 3.167 GHz and equipped with 2GB of DDR3 RAM memory. The cross-coupling between the two axes was measured to be $-40\ dB$; small enough to be neglected, thereby making it feasible to treat each axis as being decoupled from the other. Throughout the experiments, the unused axis has its input terminals shorted in order to avoid spurious excitation.

4.1. Selection of Controller Parameters

The choice of controller parameters affects the tracking performance and phase trajectory of the system. In

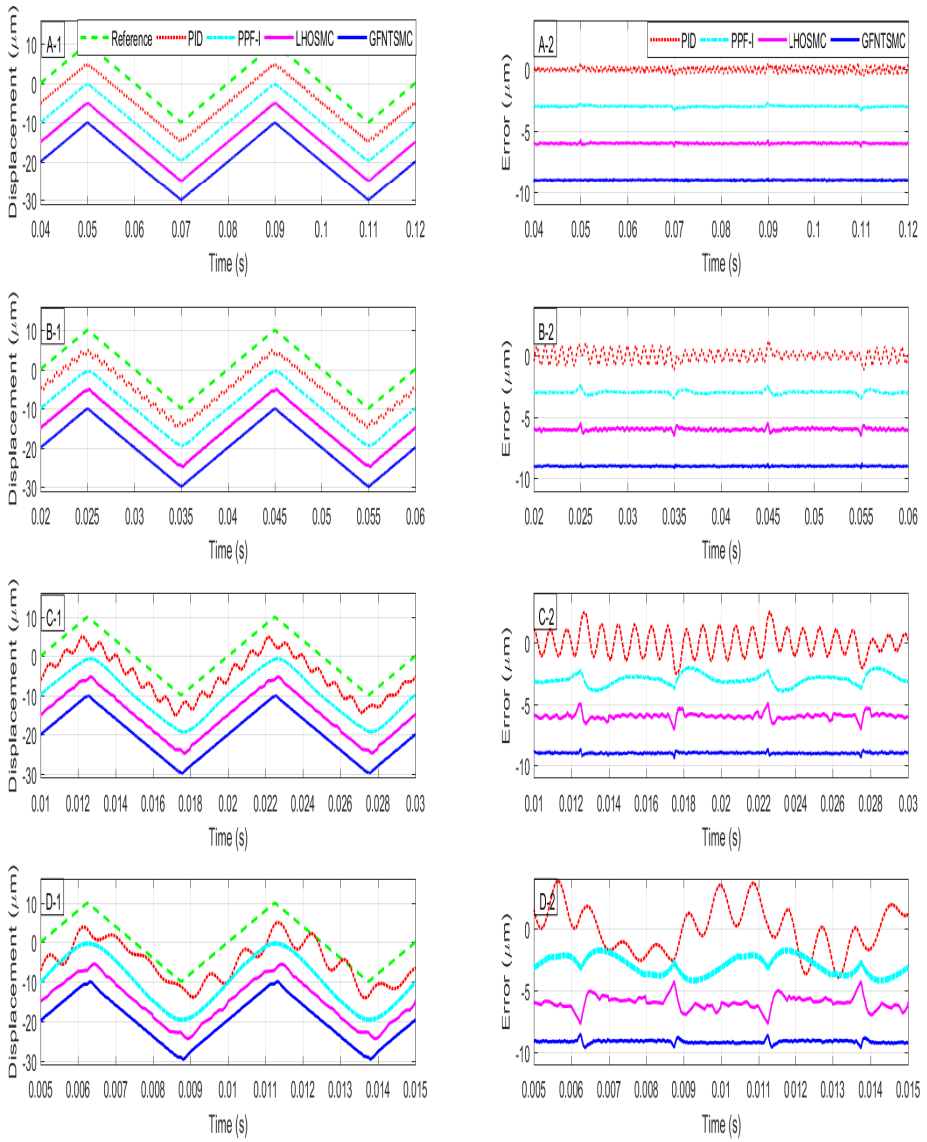

Figure 5: Closed-loop time-domain tracking results for 25 Hz, 50 Hz, 100 Hz and 200 Hz triangular reference inputs (A-1, B-1, C-1 and D-1). For clarity, the traces are offset by 5 μm. The corresponding tracking errors are plotted in (A-2, B-2, C-2 and D-2). These errors are offset by 3 μm for clarity.

the reaching phase, Eq.(15) indicates that the performance of the system is determined by parameters ϕ_1, ϕ_2, ϕ_3, λ_1, λ_2, λ_3, λ_4. The larger the value of ϕ_1, the faster the convergence. ϕ_2 controls the near equilibrium trajectory, and the higher its value, the higher the convergence accuracy. The ratio of λ_1 to λ_2 should be less than 1. A higher value of this ratio (closer to 1) results in high convergence precision and faster convergence speed (shorter time). ϕ_3 controls the stage far away from the equilibrium. The higher its value, the faster the convergence. The ratio of λ_3 to λ_4 should be greater than 1. The higher the ratio, the faster the convergence rate. In sliding phase, Eq.(8) indicates that the performance of the system is determined by parameters α, β, p_j, q_j. Constrained by the sliding Eq.(8), both α and β have to be a small value because the errors are small. α controls the system behavior far away from the equilibrium and the smaller its value, the higher is the bandwidth. A large α results in slow convergence. β controls the system behaviour near equilibrium and the smaller its value, the higher is the achieved bandwidth. If β is too small, the convergence time increases while a large value can even lead to instability. p_j and q_j are all odd numbers; the ratio between p_j to q_j has to be at least greater than $n - 1 - j$ to ensure that the control is non-singular. Moreover, a larger ratio results in higher convergence accuracy and faster convergence rate.

It should be noted that the following constraints in the control design procedure are highlighted here for the clarity of the presented results. (i) In practice, the upper

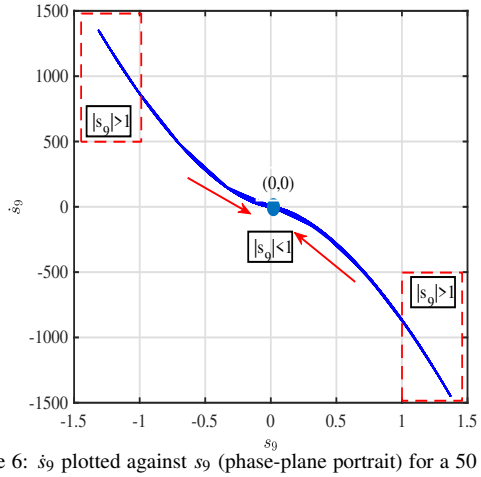

Figure 6: $\dot{s}_9$ plotted against s_9 (phase-plane portrait) for a 50 Hz triangular reference trajectory, demonstrating the proposed controller's convergence property.

bound $\bar{\Delta}$ of term Δ in Eq.(3) can usually be estimated by twice the maximum value of the tested hysteresis. (ii) All the controller parameters in Eqns. (6) and (11) should satisfy the mathematical constraints presented in the context. Using these selection principles, the control parameters obtained that deliver excellent tracking performance were found to be:

- $\alpha = 0.005, \beta = 0.0001$
- $p_0 = 129$, $p_1 = 115$, $p_2 = 103$, $p_3 = 89$, $p_4 = 77$, $p_5 = 63$, $p_6 = 51$, $p_7 = 37$, $p_8 = 25$
- $q_0 = 13$, $q_1 = 13$, $q_2 = 13$, $q_3 = 13$, $q_4 = 13$, $q_5 = 13$, $q_6 = 13$, $q_7 = 13$, $q_8 = 13$
- $\phi_1 = 20$, $\phi_2 = 20$, $\phi_3 = 20$
- $\lambda_1 = 3$, $\lambda_2 = 5$, $\lambda_3 = 9$, $\lambda_4 = 7$

It is important to note that: 1)The above selected parameters of the proposed controller are used in the experiments and simulation; 2)The parameters of the controlled plant are obtained through the identification process and the corresponding results are shown in Fig.1(b) and Fig.2; 3) The ODE5 fixed-step solver is used to implement the solution.

Using the above parameters, the phase trajectories of the controlled system can be simulated first to ascertain desired performance. Fig.6 shows the phase portrait between $\dot{s}_9$ and s_9. As the plot depicts, sliding takes place at the origin $(0, 0)$. The derivative $\dot{s}_9$ converges to a small neighborhood of zero, according to the law formalized in Eq.(14). When $|s_9| > 1$, i.e., the system moves away from the sliding surface, the third term $\phi_3 \lceil s_{n-1} \rfloor^{\lambda_3/\lambda_4} = 20 \times \lceil s_9 \rfloor^{9/7}$ plays a leading role in the convergence process. When $|s_9| < 1$, i.e., the system is approaching the sliding surface, the second term $\phi_2 \lceil s_{n-1} \rfloor^{\lambda_1/\lambda_2} = 20 \times \lceil s_9 \rfloor^{3/5}$ play a leading role in the convergence process. During the reaching phase, the system state has a fast convergence speed while going away from or approaching towards the sliding surface.

Fig.7(a) plots the time trajectories of the state variables s_n for $n = 1, 2, ...9$ while Fig.7(b) plots the time trajectory of $\dot{s}_9$ (derivative of the state variable s_9). Consider $s_j = s_{j-1} + \alpha \lceil s_{j-1} \rfloor^{p_{j-1}/q_{j-1}} + \beta \dot{s}_{j-1}$ for example. When $s_j = 0$, then $\dot{s}_{j-1} = -\frac{1}{\beta} s_{j-1} - \frac{\alpha}{\beta} \lceil s_{j-1} \rfloor^{p_{j-1}/q_{j-1}}$. When $|s_{j-1}| > 1$, which indicates that the system is away from the equilibrium point, the second term $-\frac{\alpha}{\beta} \lceil s_{j-1} \rfloor^{p_{j-1}/q_{j-1}}$ plays a leading role in determining the convergence speed, because $p_{j-1}/q_{j-1} > 1$ as shown in Fig.7(a). When $|s_{j-1}| < 1$, which means the system is approaching the equilibrium point, the first term $-\frac{1}{\beta} s_{j-1}$ play a leading role in the convergence process, because $1 < p_{j-1}/q_{j-1}$, as shown in Fig.7(a). Moreover, it is evident from Fig.7(b) that $\dot{s}_9$ converges very steeply and goes to equilibrium rapidly at each discontinuous point (corner) of the triangular wave. As s_9 converges to a small neighborhood of zero, s_8, s_7, s_6, ... s_1 will sequentially converge to a small neighborhood of zero according to the law given in Eqn 8, as shown in Fig.7(a).

Therefore, from Fig.6 and Fig.7, it can be concluded that irrespective of where the initial state of the system is located in the phase-plane, the proposed sliding mode control scheme can always drive the system state to the equilibrium point quickly. In other words, it can reach the equilibrium point quickly in both the sliding stage and the reaching stage. The global fast convergence is demonstrated. So, we can conclude that the change of initial conditions has little effect on the system tracking performance.

4.2. Tracking performance - Comparative analysis

As we know, the nanopositioner is a very complex plant to be controlled mainly due to its nonlinear hysteresis as well as the high-bandwidth dynamics. In order to verify the positioning performance of the proposed controller, triangular trajectories with fundamental frequencies of 25 Hz, 50 Hz, 100Hz and 200 Hz were chosen. To compare the positioning performance of the proposed controller, the maximum (MAX) as well as root-mean-square (RMS) tracking errors obtained were compared with three suitably designed control schemes that have emerged as benchmark over the years. The first scheme is a simple PID controller. The individual gains are tuned to results in maximum positioning bandwidth. The second control scheme is the popularly employed

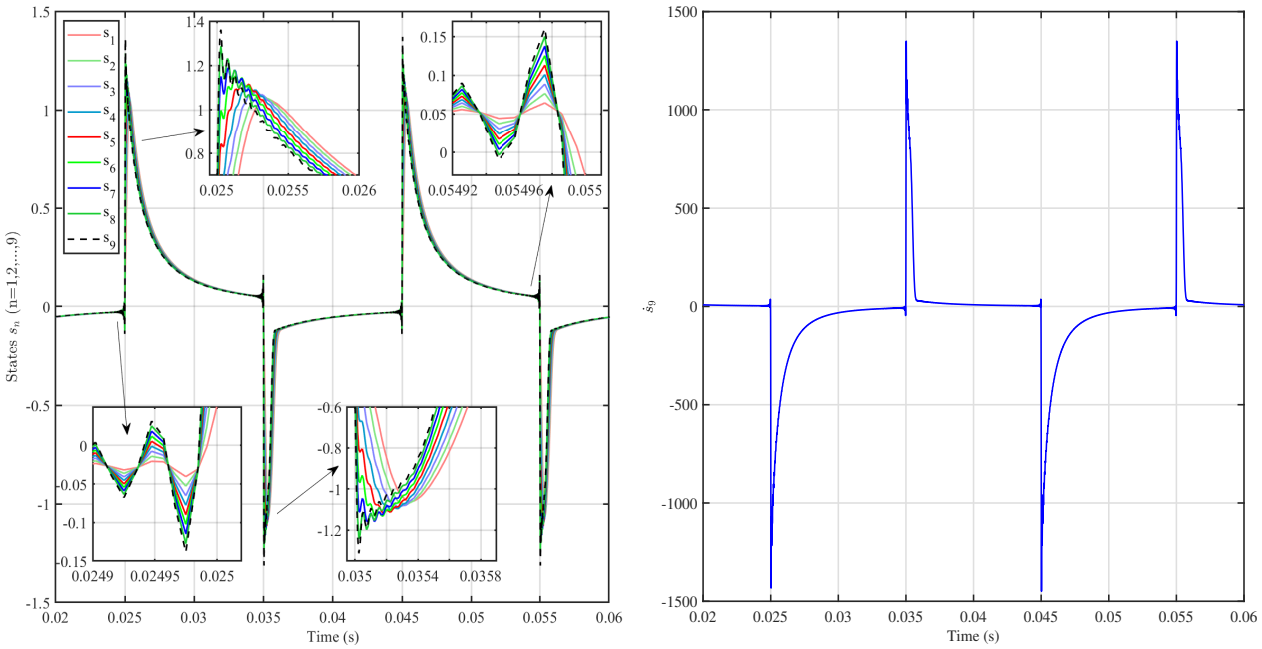

(a) (b)

Figure 7: (a) The evolution of state variables vs time. (b) The evolution of $\dot{s}_9$ versus time.

combination of damping and tracking actions where an inner-loop damping controller is implemented in tandem with a tracking controller in the outer loop [54]. Due to its popularity and excellent performance, the Positive Position Feedback (PPF) damping controller compined with an Integral (I) tracking controller was employed. The third one is a well-tuned traditional linear high-order sliding mode controller (LHOSMC).

The three parameters of PID controller were found to be: $K_P = 1.5$, $K_I = 6500$, $K_D = 0.0005$. In fact, irrespective of the tuning, the overall positioning bandwidth of the PID control scheme will be severely limited due to the undamped resonant mode of the nanopositioner. This fact can be found and supported by a lot of literature [55, 56]. To overcome this limitation, many other control schemes have been used. For example, the well-known scheme [57, 41, 58] which combines damping and tracking controllers can deliver superior positioning performance (due to the application of a higher gain tracking controller) than the PID alone. In this paper, the transfer function for the designed PPF damping controller is given by:

$$C_{PPF} = \frac{6.320 \times 10^7}{s^2 + 11740s + 4.855 \times 10^7} \tag{25}$$

and the corresponding integral gain implemented is $K_I = 1490$. A LHOSMC controller [59] is adopted in this work, and it is modified with equivalent and switching control actions. The experimentally recorded time-domain tracking results are presented in Fig.5. The resulting errors are presented in Table 1.

Table 1: Maximum and RMS tracking errors of the 4 control schemes.

Error (μm)	Frequency (Hz)	Controller			
		Proposed	LHOSMC	PPF-I	PID
MAX	25	1.06	1.84	1.94	3.40
	50	2.09	3.26	3.35	6.38
	100	2.47	5.05	5.12	13.35
	200	3.25	9.15	11.25	40.05
RMS	25	0.26	0.35	0.37	1.05
	50	0.57	0.60	0.64	2.43
	100	1.14	2.23	2.29	4.46
	200	2.10	4.12	4.85	13.04

It is evident from the error analysis in Table 1, as well as the time-domain plots in Fig.5 A-2, B-2, C-2 and D-2; that the proposed GNFTSMC scheme delivers a significantly superior performance when compared to the standard PID or the popular PPF with Integral action schemes. From Fig.5 and Table 1, we can see the tracking performance of the proposed controller is

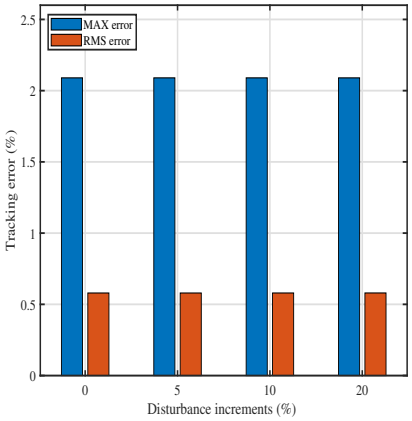

Figure 8: Bar chart for tracking errors plotted against parameter uncertainty included as a disturbance in percentage increments, for 50 Hz reference trajectory.

significantly improved, especially at higher frequencies of scan trajectories where the errors are reduced to less than 50% of those achieved by PPF-I. It must be noted that high-frequency nanopositioning is the current need and thus this error reduction is significant enough to motivate the application of this seemingly evolved control scheme. In order to conduct a relatively fair comparison with the conventional SMC, a LHOSMC has been compared and from the results we can see the well-tuned LHOSMC can not reach satisfactory performance, especially in high frequency. The tracking precision decreases a lot with the increase of bandwidth. To ensure that the proposed control scheme has robustness built-in, it was tested against a series of incremental changes to the model parameters, treated as disturbance Δ.

4.3. Robustness verification

Robustness to system parameter uncertainty was evaluated by adding an incremental disturbance (in percentage) to all the model parameters a_n by $\varepsilon \times a_n$. $(n = 0, 1, 2, ...9)$ as given in Eq.1. Consequently, all a_n are simultaneously increased by ε. Here, ε is selected as 0%, 5%, 10%, 20%. The 50 Hz triangular trajectory is used as a reference throughout this analysis. Figure 8 plots the maximum and RMS tracking errors in percentage against increasing values of disturbance in percentages. It is seen that the tracking errors remain virtually unchanged.

Fig.9 shows the corresponding control actions for different disturbance levels. Note that the key parameter uncertainty lies in the change in the frequency and damping of the dominant first resonant mode - a direct consequence of change in the scanned specimen, which

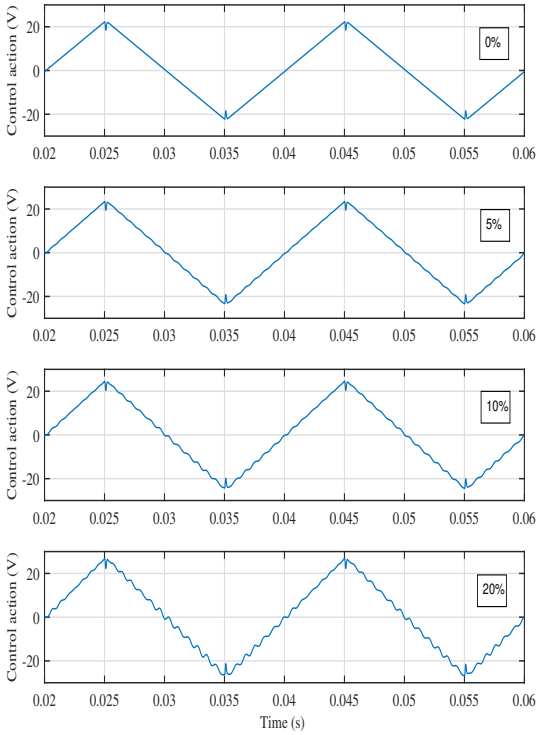

Figure 9: A trace of the steady-state control actions while tracking a 50 Hz triangular reference trajetory, for 0%, 5%, 10% and 20% change in all system parameters a_n of the open-loop model of the linear dynamics of the system, given in Eq.1.

results in a change in mass (reducing the overall resonant frequency of the axis $\omega_{res} = \sqrt{\frac{k}{m}}$ where k is the spring constant and m is the equivalent mass). As the disturbance increases, the control signal varies in frequency content (as evidenced by the increased ripple) to accommodate for the change in resonance and a slight change in amplitude to accommodate for the slight variation in the input-to-output gain of the system. However, the system experiences no chattering or instability issues as evidenced by the smooth steady-state control inputs plotted here.

5. Conclusions

A new Global Fast Non-singular Terminal Sliding-Mode Control (GFNTSMC) scheme has been presented for a piezoelectric platform in this paper. The stability of the proposed scheme is proved using the classical Lyapunov framework. Experimental comparison

of the tracking results delivered by the proposed GN-FTSMC scheme against that delivered by the standard PID and the popular PPF with Integral control schemes demonstrates the superior performance afforded by the proposed scheme. The proposed scheme possesses excellent robustness over a wide variation in parameter values. Moreover, the control structure is such that the tracking errors are almost independent of the parameter uncertainty as long as there is sufficient input range available. This required change in control input is by no means prohibitive. An optimal method searching for the best combination of controller parameters will be investigated in the future.

Declaration of Competing Interest

The authors declare that they have no known competing financial interests or personal relationships that could have appeared to influence the work reported in this paper.

Appendix

$$\frac{d^n}{dt^n}\lceil s\rfloor^r = \sum_{\theta=0}^{n-1}\left[\prod_{k=0}^{\theta}(r-k)*\lceil s\rfloor^{r-\theta-1}*\sum_{j=1}^{C_{n-1}}T_j^{\theta}\right] \tag{26}$$

where, $T_j^{\theta} = s^{(a_1)}*s^{(a_2)}*s^{(a_3)}*\cdots*s^{(a_{\theta+1})}*\frac{\prod_{i=1}^{\theta+1}C_{n-}^{a_i}}{A_{\theta+1}^{\theta}}$, $a_0 = 0, a_i \in N^+$, and $\sum a_i = n$. $r > n$ and it is the ratio of two positive odd numbers. A and C are symbols of permutation and combination, respectively.

Proof. The induction method is used to prove the above results. The first 5 derivatives of $\lceil s\rfloor^r$ are very simple, and thus can be used to easily verify the above results. They are omitted here. For the n-th derivatives of $\lceil s\rfloor^r$, we assume that the Eq.(26) holds. Then, for arbitrary θ ($\theta \neq 0$), $\frac{d^n}{dt^n}\lceil s\rfloor^r$ includes the following general component denoted as M:

$$M = \prod_{k=0}^{\theta-1}(r-k)*\lceil s\rfloor^{r-(\theta-1)-1}*\sum_{j=1}^{C_{n-1}^{\theta-1}}T_j^{\theta-1}+$$

$$\prod_{k=0}^{\theta}(r-k)*\lceil s\rfloor^{r-\theta-1}*\sum_{j=1}^{C_{n-1}^{\theta}}T_j^{\theta}$$

Then we have

$$\frac{d}{dt}M = \prod_{k=0}^{\theta-1}(r-k)*(r-\theta)*\lceil s\rfloor^{r-\theta-1}*\frac{d}{dt}s*\sum_{j=1}^{C_{n-1}^{\theta-1}}T_j^{\theta-1}+$$

$$\prod_{k=0}^{\theta-1}(r-k)*\lceil s\rfloor^{r-(\theta-1)-1}*\frac{d}{dt}\left(\sum_{j=1}^{C_{n-1}^{\theta-1}}T_j^{\theta-1}\right)+$$

$$\prod_{k=0}^{\theta}(r-k)*(r-\theta-1)*\lceil s\rfloor^{r-\theta-2}*\frac{d}{dt}s*\sum_{j=1}^{C_{n-1}^{\theta}}T_j^{\theta}+$$

$$\prod_{k=0}^{\theta}(r-k)*\lceil s\rfloor^{r-\theta-1}*\frac{d}{dt}\left(\sum_{j=1}^{C_{n-1}^{\theta}}T_j^{\theta}\right)$$

$$=\prod_{k=0}^{\theta-1}(r-k)*\lceil s\rfloor^{r-\theta}*\frac{d}{dt}\left(\sum_{j=1}^{C_{n-1}^{\theta-1}}T_j^{\theta-1}\right)$$

$$\prod_{k=0}^{\theta}(r-k)*\lceil s\rfloor^{r-\theta-1}*\left[\frac{d}{dt}\left(\sum_{j=1}^{C_{n-1}^{\theta}}T_j^{\theta}\right)+\frac{d}{dt}s*\sum_{j=1}^{C_{n-1}^{\theta-1}}T_j^{\theta-1}\right]+$$

$$\prod_{k=0}^{\theta}(r-k)*(r-\theta-1)*\lceil s\rfloor^{r-\theta-2}*\frac{d}{dt}s*\sum_{j=1}^{C_{n-1}^{\theta}}T_j^{\theta}$$

And from the expression of T_j^{θ}, we can get

$$\frac{d}{dt}\left(\sum_{j=1}^{C_{n-1}^{\theta}}T_j^{\theta}\right)+\frac{d}{dt}s*\sum_{j=1}^{C_{n-1}^{\theta-1}}T_j^{\theta-1}=\sum_{j=1}^{C_n^{\theta}}T_j^{\theta}$$

Therefore, as for the second term of $\frac{d}{dt}M$, we have

$$\prod_{k=0}^{\theta}(r-k)*\lceil s\rfloor^{r-\theta-1}*\left[\frac{d}{dt}\left(\sum_{j=1}^{C_{n-1}^{\theta}}T_j^{\theta}\right)+\frac{d}{dt}s*\sum_{j=1}^{C_{n-1}^{\theta-1}}T_j^{\theta-1}\right]=$$

$$\prod_{k=0}^{\theta}(r-k)*\lceil s\rfloor^{r-\theta-1}*\sum_{j=1}^{C_n^{\theta}}T_j^{\theta} \tag{27}$$

Obviously, the right hand of the above Eq.(27) is one general component of $\frac{d^{n+1}}{dt^{n+1}}\lceil s\rfloor^n$. Then, we can conclude that, as long as Eq.(26) holds, the following formula holds

$$\frac{d^{n+1}}{dt^{n+1}}\lceil s\rfloor^r = \frac{d}{dt}\left[\frac{d^n}{dt^n}\lceil s\rfloor^r\right]$$

$$=\sum_{\theta=0}^{n}\left[\prod_{k=0}^{\theta}(r-k)*\lceil s\rfloor^{r-\theta-1}*\sum_{j=1}^{C_m^{\theta}}T_j^{\theta}\right]$$

It should be note that the above result also holds under the condition that $\frac{d}{dt}s*\sum_{j=1}^{C_{n-1}^{\theta-1}}T_j^{\theta-1}=0$ when $\theta=0$.

Proof is completed. □

References

[1] Y. Zhang, P. Yan, Z. Zhang, Frequency-shaped sliding mode control of piezoelectric nano-stages with hysteresis estimation, ISA Transactions-doi:https://doi.org/10.1016/j.isatra.2020.08.002.

[2] S. Yu, M. Xie, H. Wu, J. Ma, Y. Li, H. Gu, Composite proportional-integral sliding mode control with feedforward control for cell puncture mechanism with piezoelectric actuation, ISA transactions.

[3] G. Wang, Q. Xu, Design and precision position/force control of a piezo-driven microinjection system, IEEE/ASME Transactions on Mechatronics 22 (4) (2017) 1744–1754.

[4] E. Csencsics, B. Sitz, G. Schitter, Integration of Control Design and System Operation of a High Performance Piezo-Actuated Fast Steering Mirror, IEEE/ASME Transactions on Mechatronics 25 (1) (2020) 239–247. doi:10.1109/TMECH.2019.2959087.

[5] J. Li, H. Tang, Z. Wu, H. Li, G. Zhang, X. Chen, J. Gao, Y. Xu, Y. He, A Stable Autoregressive Moving Average Hysteresis Model in Flexure Fast Tool Servo Control, IEEE Transactions on Automation Science and Engineering 16 (3) (2019) 1484–1493. doi:10.1109/TASE.2019.2899342.

[6] L. Liu, H. Yun, Q. Li, X. Ma, S.-L. Chen, J. Shen, Fractional Order Based Modeling and Identification of Coupled Creep and Hysteresis Effects in Piezoelectric Actuators, IEEE/ASME Transactions on Mechatronics 25 (2) (2020) 1036–1044. doi:10.1109/TMECH.2020.2974978.

[7] S. Kang, M. G. Lee, Y.-M. Choi, Six Degrees-of-Freedom Direct-Driven Nanopositioning Stage Using Crab-Leg Flexures, IEEE/ASME Transactions on Mechatronics 25 (2) (2020) 513–525. doi:10.1109/TMECH.2020.2972301.

[8] D. Habineza, M. Zouari, Y. Le Gorrec, M. Rakotondrabe, Multivariable Compensation of Hysteresis, Creep, Badly Damped Vibration, and Cross Couplings in Multiaxes Piezoelectric Actuators, IEEE Transactions on Automation Science and Engineering 15 (4) (2018) 1639–1653. doi:10.1109/TASE.2017.2772221.

[9] P. R. N. Tuwa, P. Woafo, Suppression of the noise-induced effects in an electrostatic micro-plate using an adaptive backstepping sliding mode control, ISA TRANSACTIONS 72 (2018) 100–109. doi:10.1016/j.isatra.2017.10.003.

[10] A. San-Millan, V. Feliu-Batlle, S. S. Aphale, Two-degrees-of-freedom (PID)-D-2 controller for precise nanopositioning in the presence of hardware-induced constant time delay, ISA TRANSACTIONS 91 (2019) 207–217. doi:10.1016/j.isatra.2019.01.028.

[11] Y. Liu, Y. Wang, X. Chen, Online hysteresis identification and compensation for piezoelectric actuators, IEEE Transactions on Industrial Electronics 67 (7) (2020) 5595–5603.

[12] A. San-Millan, D. Russell, V. Feliu, S. S. Aphale, A modified positive velocity and position feedback scheme with delay compensation for improved nanopositioning performance, Smart Materials and Structures 24 (7) (2015) 075021.

[13] X. Zhang, X. Chen, G. Zhu, C. Su, Output feedback adaptive motion control and its experimental verification for time-delay nonlinear systems with asymmetric hysteresis, IEEE Transactions on Industrial Electronics 67 (8) (2020) 6824–6834.

[14] M. Altaher, D. Russell, S. S. Aphale, A dual-loop tracking control approach to precise nanopositioning, Journal of Vibration and Control 25 (3) (2019) 666–674.

[15] J. Y. Lau, W. Liang, K. K. Tan, Adaptive sliding mode enhanced disturbance observer-based control of surgical device, ISA TRANSACTIONS 90 (2019) 178–188. doi:10.1016/j.isatra.2018.12.048.

[16] A. Safa, R. Y. Abdolmalaki, S. Shafiee, B. Sadeghi, Adaptive nonsingular terminal sliding mode controller for micro/nanopositioning systems driven by linear piezoelectric ceramic motors, ISA TRANSACTIONS 77 (2018) 122–132. doi:10.1016/j.isatra.2018.03.027.

[17] Y. Zhang, P. Yan, An adaptive integral sliding mode control approach for piezoelectric nano-manipulation with optimal transient performance, Mechatronics 52 (2018) 119–126.

[18] K.-B. Park, T. Tsuji, Terminal sliding mode control of second-order nonlinear uncertain systems, International Journal of Robust and Nonlinear Control 9 (11) (1999) 769–780.

[19] Y. Feng, X. Yu, Z. Man, Non-singular terminal sliding mode control of rigid manipulators, Automatica 38 (12) (2002) 2159–2167.

[20] A. Al-Ghanimi, J. Zheng, Z. Man, Robust and fast non-singular terminal sliding mode control for piezoelectric actuators, IET Control Theory & Applications 9 (18) (2015) 2678–2687.

[21] L. Yang, J. Yang, Nonsingular fast terminal sliding-mode control for nonlinear dynamical systems, International Journal of Robust and Nonlinear Control 21 (16) (2011) 1865–1879.

[22] J. Zheng, H. Wang, Z. Man, J. Jin, M. Fu, Robust motion control of a linear motor positioner using fast nonsingular terminal sliding mode, IEEE/ASME Transactions on Mechatronics 20 (4) (2015) 1743–1752.

[23] J. P. Mishra, Q. Xu, X. Yu, M. Jalili, Precision Position Tracking for Piezoelectric-Driven Motion System Using Continuous Third-Order Sliding Mode Control, IEEE/ASME Transactions on Mechatronics 23 (4) (2018) 1521–1531. doi:10.1109/TMECH.2018.2853737.

[24] G. Wang, Q. Xu, Adaptive terminal sliding mode control for motion tracking of a micropositioning system, Asian Journal of Control 20 (3) (2018) 1241–1252.

[25] Q. Xu, Precision Motion Control of Piezoelectric Nanopositioning Stage With Chattering-Free Adaptive Sliding Mode Control, IEEE Transactions on Automation Science and Engineering 14 (1) (2017) 238–248. doi:10.1109/TASE.2016.2575845.

[26] X. Yu, Y. Wu, Z. H. Man, On global stabilization of nonlinear dynamical systems, in: Variable structure systems, sliding mode and nonlinear control, Springer, 1999, pp. 109–122.

[27] X. Yu, Z. H. Man, Fast terminal sliding-mode control design for nonlinear dynamical systems, IEEE Transactions on Circuits and Systems I: Fundamental Theory and Applications 49 (2) (2002) 261–264.

[28] G.-Y. Gu, L.-M. Zhu, C.-Y. Su, H. Ding, S. Fatikow, Modeling and control of piezo-actuated nanopositioning stages: A survey, IEEE Transactions on Automation Science and Engineering 13 (1) (2016) 313–332.

[29] Z. Wang, Z. Zhang, J. Mao, Precision tracking control of piezoelectric actuator based on bouc-wen hysteresis compensator, Electronics letters 48 (23) (2012) 1459–1460.

[30] M. Rakotondrabe, Bouc–wen modeling and inverse multiplicative structure to compensate hysteresis nonlinearity in piezoelectric actuators, IEEE Transactions on Automation Science and Engineering 8 (2) (2010) 428–431.

[31] G. Sun, Z. Ma, Practical tracking control of linear motor with adaptive fractional order terminal sliding mode control, IEEE/ASME Transactions on Mechatronics 22 (6) (2017) 2643–2653. doi:10.1109/TMECH.2017.2766279.

[32] S. Kamal, J. A. Moreno, A. Chalanga, B. Bandyopadhyay, L. M. Fridman, Continuous terminal sliding-mode controller, Automatica 69 (2016) 308–314.

[33] G. Marks, Y. Shtessel, H. Gratt, I. Shkolnikov, Effects of high order sliding mode guidance and observers on hit-to-kill interceptions, in: AIAA guidance, navigation, and control conference and exhibit, 2005, p. 5967.

[34] M. Abramowitz, I. A. Stegun, R. H. Romer, Handbook of mathematical functions with formulas, graphs, and mathematical tables (1988).

[35] Y. S. Lu, J. S. Chen, Design of a global sliding-mode controller for a motor drive with bounded control, International Journal of Control 62 (5) (1995) 1001–1019.

[36] Y. Zhu, J. Fei, Adaptive global fast terminal sliding mode control of grid-connected photovoltaic system using fuzzy neural network approach, IEEE Access 5 (2017) 9476–9484.

[37] J. J. Xiong, G. B. Zhang, Global fast dynamic terminal sliding mode control for a quadrotor uav, ISA Transactions 66 (2016) 233–240.

[38] A. San-Millan, S. S. Aphale, V. Feliu, A fast algebraic estimator for system parameter estimation and online controller tuning—a nanopositioning application, IEEE Transactions on Industrial Electronics 66 (6) (2019) 4534–4543. doi:10.1109/TIE.2018.2863206.

[39] A. San-Millan, V. Feliu-Batlle, S. S. Aphale, Fractional order implementation of integral resonant control–a nanopositioning application, ISA transactions 82 (2018) 223–231.

[40] M. Altaher, S. S. Aphale, High-precision control of a piezo-driven nanopositioner using fuzzy logic controllers, Computers 7 (1) (2018) 10.

[41] S. R. Moheimani, Invited review article: Accurate and fast nanopositioning with piezoelectric tube scanners: Emerging trends and future challenges, Review of Scientific Instruments 79 (7) (2008) 071101.

[42] S. P. Wadikhaye, Y. K. Yong, B. Bhikkaji, S. R. Moheimani, Control of a piezoelectrically actuated high-speed serial-kinematic afm nanopositioner, Smart materials and structures 23 (2) (2014) 025030.

[43] E. Pereira, S. S. Aphale, V. Feliu, S. R. Moheimani, Integral resonant control for vibration damping and precise tip-positioning of a single-link flexible manipulator, IEEE/ASME Transactions on Mechatronics 16 (2) (2010) 232–240.

[44] Q. Zhang, Y. Dong, Y. Peng, J. Luo, S. Xie, H. Pu, Asymmetric bouc–wen hysteresis modeling and inverse compensation for piezoelectric actuator via a genetic algorithm–based particle swarm optimization identification algorithm, Journal of Intelligent Material Systems and Structures 30 (8) (2019) 1263–1275.

[45] F. Stefanski, B. Minorowicz, J. Persson, A. Plummer, C. Bowen, Non-linear control of a hydraulic piezo-valve using a generalised prandtl–ishlinskii hysteresis model, Mechanical Systems and Signal Processing 82 (2017) 412–431.

[46] L. Zhu, W. Wu, X. Xu, Y. Guo, W. Li, K. Lu, C.-S. Koh, An improved anisotropic vector preisach hysteresis model taking account of rotating magnetic fields, IEEE Transactions on Magnetics 55 (6) (2019) 1–4.

[47] A. San-Millan, D. Russell, V. Feliu, S. S. Aphale, A modified positive velocity and position feedback scheme with delay compensation for improved nanopositioning performance, Smart Materials and Structures 24 (7) (2015) 075021.

[48] Q. Xu, Adaptive integral terminal third-order finite-time sliding-mode strategy for robust nanopositioning control, IEEE Transactions on Industrial Electronics (2020) 1–1doi:10.1109/TIE.2020.2998751.

[49] J. P. Mishra, Q. Xu, X. Yu, M. Jalili, Precision position tracking for piezoelectric-driven motion system using continuous third-order sliding mode control, IEEE/ASME Transactions on Mechatronics 23 (4) (2018) 1521–1531. doi:10.1109/TMECH.2018.2853737.

[50] L.-J. Lai, G.-Y. Gu, L.-M. Zhu, Design and control of a decoupled two degree of freedom translational parallel micro-positioning stage, Review of Scientific Instruments 83 (4) (2012) 045105.

[51] Q. Wang, Q. Xu, Fpga based adaptive sliding mode control of a piezoelectric-driven micropositioning system, in: 2017 IEEE 7th Annual International Conference on CYBER Technology in Automation, Control, and Intelligent Systems (CYBER), 2017, pp. 1147–1152. doi:10.1109/CYBER.2017.8446607.

[52] Z. Nan, Q. Xu, S. Li, Design and testing of a new high-order integral terminal sliding mode controller, in: 2019 Chinese Control Conference (CCC), 2019, pp. 2611–2616. doi:10.23919/ChiCC.2019.8865888.

[53] G. Wang, Q. Xu, Sliding mode control with disturbance rejection for piezoelectric nanopositioning control, in: 2018 Annual American Control Conference (ACC), 2018, pp. 6144–6149. doi:10.23919/ACC.2018.8431754.

[54] D. Russell, A. J. Fleming, S. S. Aphale, Simultaneous optimization of damping and tracking controller parameters via selective pole placement for enhanced positioning bandwidth of nanopositioners, Journal of Dynamic Systems, Measurement, and Control 137 (10).

[55] A. J. Fleming, Nanopositioning system with force feedback for high-performance tracking and vibration control, IEEE/Asme Transactions on Mechatronics 15 (3) (2010) 433–447.

[56] K. K. Leang, S. Devasia, Feedback-linearized inverse feedforward for creep, hysteresis, and vibration compensation in afm piezoactuators, IEEE Transactions on Control Systems Technology 15 (5) (2007) 927–935.

[57] S. Devasia, E. Eleftheriou, S. R. Moheimani, A survey of control issues in nanopositioning, IEEE Transactions on Control Systems Technology 15 (5) (2007) 802–823.

[58] A. J. Fleming, S. S. Aphale, S. R. Moheimani, A new method for robust damping and tracking control of scanning probe microscope positioning stages, IEEE Transactions on Nanotechnology 9 (4) (2009) 438–448.

[59] A. Levant, Higher-order sliding modes, differentiation and output-feedback control, International journal of Control 76 (9-10) (2003) 924–941.